COMMUNICATION

Check for updates

A Pd-labile fluoroquinolone prodrug efficiently prevents biofilm formation on coated surfaces†

Josef Braun,[a] M. Carmen Ortega-Liebana, [ID] [b,c,d,e,f] Asier Unciti-Broceta [ID] [b,c] and Stephan A. Sieber [ID] *[a]

Surface-adhered bacteria on implants represent a major challenge for antibiotic treatment. We introduce hydrogel-coated surfaces loaded with tailored Pd-nanosheets which catalyze the release of antibiotics from inactive prodrugs. Masked and antibiotically inactive fluoroquinolone analogs were efficiently activated at the surface and prevented the formation of *Staphylococcus aureus* biofilms.

Biomedical implants such as prosthetics and catheters represent an important breakthrough in modern medicine to ease patients' lives. However, these implants can be associated with bacterial infections *e.g.* caused by *Staphylococcus aureus* that colonize the surface and build biofilms that are difficult to eradicate. Biofilms are composed of surface-adhered bacteria shielded by an extracellular polymeric matrix effectively preventing the penetration of small molecules such as antibiotics. The release of bacteria from the biofilm into the surrounding tissue is a constant source for relapsing infections and usually requires a full surgical replacement of the implant.[1] For these reasons, biofilms represent a major challenge for drug treatment and account for up to 25% of health-care associated infections in the USA.[2] Currently, only a few drugs such as rifampicin and ciprofloxacin are used to treat biofilms, requiring high dosage and resulting in limited success rates.[2–4] In

addition, a high dosage of some antibiotics such as ciprofloxacin can lead to severe side effects preventing further treatment.[5] Despite this high unmet medical need, the discovery pipeline for new anti-biofilm drugs is rather empty.[6,7] Until potent drugs are discovered, intermediate treatment solutions are desperately needed. One strategy focuses on anti-microbial coatings of the implant preventing the association of biofilms by the slow and constant release of antibiotics.[8] While such a strategy is powerful for preventing infections after the surgery, consumption of the antibiotic enhances the risk of reoccurring infections. Another so far little exploited strategy is based on prodrugs bearing a masked, non-toxic scaffold that is activated at the site of biofilm formation. The advantage is that these non-toxic molecules can be applied at high concentrations, however, a specific cleavage of the prodrug at the location of the biofilm is needed. Here, differences in pH or cleavage by enzymes led to controlled release of antibiotics in the vicinity of the biofilm.[9–11] A related strategy has been explored by Rotello using prodrugs that are activated by Fe(III) catalysis, yielding catalytic nanodevices that directly penetrate biofilms.[12–14] A yet largely unexplored strategy is the prodrug cleavage directly at the implant surface pioneered by immobilized enzymes.[10] Ideally, a surface coating is stable, not consumed over time and can react in an infinite number of catalytic cycles. Such a prodrug mediated cleavage on bioimplant surfaces requires a compatible design of the compound, the coating and the catalyst. In this direction, biorthogonal catalytic reactions, such as depropargylation reactions catalyzed by Pd or Au, have found application for the local activation of a variety of FDA-approved drugs, including anticancer drugs and antidepressants.[15–24]

Inspired by these advances, here we exploit metal catalyzed prodrug release on implant surfaces based on Pd nanoparticles embedded in hydrogel coatings. Propargylated fluoroquinolone prodrugs were synthesized and upon cleavage on Pd-nanosheets led to prevention of *S. aureus* biofilm formation on coated surfaces. With Pd(0) nanosheets (PdNS) as tailored catalyst, we selected hydrogels as candidate coatings due to

[a]*Technical University of Munich, TUM School of Natural Sciences, Department of Bioscience, Center for Functional Protein Assemblies (CPA), Ernst-Otto-Fischer Strasse 8, 85748 Garching bei München, Germany. E-mail: stephan.sieber@tum.de*
[b]*Edinburgh Cancer Research, Institute of Genetics and Cancer, University of Edinburgh, EH4 2XR Edinburgh, UK*
[c]*CRUK Scotland Centre, UK*
[d]*Department of Medicinal & Organic Chemistry and Unit of Excellence in Chemistry Applied to Biomedicine and the Environment, Faculty of Pharmacy, University of Granada, 18071 Granada, Spain*
[e]*GENYO, Pfizer/University of Granada/Andalusian Regional Government, PTS Granada, 18016 Granada, Spain*
[f]*Instituto de Investigación Biosanitaria ibs. GRANADA, Granada, Spain*
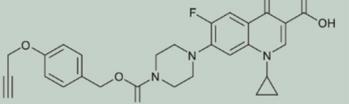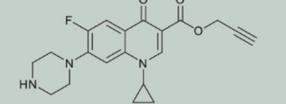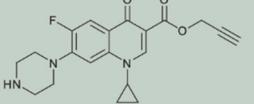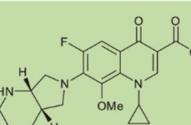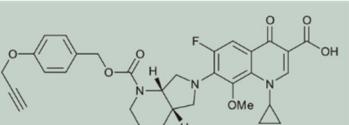
1998 | *Org. Biomol. Chem.*, 2024, **22**, 1998–2002

This journal is © The Royal Society of Chemistry 2024

their proven record as biocompatible scaffolds for bioorthogonal catalysis and antibacterial implant coatings.[18,25]

To test if this strategy works for preventing biofilm formation, we selected fluoroquinolones ciprofloxacin and moxifloxacin which are usually used at high concentrations to treat biofilms and are known to exhibit side effects (Fig. 1A). We equipped ciprofloxacin with an alkyne functionality either directly at the acid moiety or with a self-immolative linker at its secondary amino position leading to prodrugs Cipro-Pro 1 and Cipro-Pro 2, respectively. In addition, moxifloxacin was modified at its secondary amine-group yielding novel prodrug Moxi-Pro 1. In comparison to the parent compounds prodrugs Cipro-Pro 2 and Moxi-Pro 1 did not show any pronounced antibiotic activity as expressed by their minimal inhibitory concentration (MIC) against *S. aureus* and *E. coli* (Fig. 1B). In contrast, N-terminally modified ciprofloxacin (Cipro-Pro 1) largely retained antibiotic activity and was thus excluded from further studies.

In agreement with the MIC results, the minimal biofilm inhibitory concentration (MBIC) against *S. aureus* was significantly impaired by the prodrugs with 8- to over 60-fold reduced potency for Cipro-Pro 2 and Moxi-Pro 1, respectively (Fig. 1B). No acute toxicity for any compound was observed against HepG2 cells (Fig. S1†). Therefore, Cipro-Pro 2 and Moxi-Pro 1 were progressed to the next stage of the project.

By using tungsten hexacarbonyl ($W(CO)_6$) as a reducing agent, uniform and well-defined Pd nanosheets (PdNS) were successfully synthesized. In order to study the catalytic performance with respect to the optimal size of the nanostructures, we fabricated two different sized PdNS in high yield by varying the amounts of citric acid (CA) fed in the procedure (see the Experimental section for details). The size of PdNS decreased by increasing the amount of CA as observed by transmission electron microscopy (TEM) (Fig. 2A) and high-angle annular dark-field scanning transmission electron microscopy (HAADF-STEM) image (Fig. 2B). From these TEM images, the average edge length of the PdNS decreased from 17.4 to 9.1 nm with increasing amounts of CA from 90 to 170 mg, named PdNS-90 and PdNS-170, respectively (Fig. 2, and Fig. S2†). These data were obtained from 300 PdNS randomly selected from TEM images. The use of CA accelerates the reduction rate by forming a strong complex with the reduced W^{6+} ion species.[26] Thus, the edge length of the PdNS decreased with increasing amount of CA due to faster nucleation. During the reaction, $W(CO)_6$ decomposes into W particles and carbon monoxide (CO) which act reducing and capping agents in the synthesis of Pd nanosheets, respectively.[27] The poly-(vinylpyrrolidone) (PVP) serves as a stabilizing agent, and the Br^- ions control the homogeneous growth of the nanosheets. We used the energy-dispersive X-ray spectroscopy (EDS) to characterize the chemical composition of the obtained PdNS. The energy dispersive X-ray spectroscopy (EDS) elemental mapping of the PdNS vertically oriented on the TEM


Fig. 1 Pd-labile prodrugs of fluoroquinolones. (A) Structures of the parent antibiotics and corresponding Pd-labile prodrugs developed in this study. (B) Minimal Inhibitory Concentrations (MIC) and Minimal Biofilm Inhibitory Concentrations (MBIC) of the prodrugs and their parent antibiotics.

	MIC [μM] *E. coli* UTI89	MIC [μM] *S. aureus* SA113	MBIC [μM] *S. aureus* SA113
Ciprofloxacin	0.03	0.63	1.25
Cipro-Pro 1	0.03	0.63	-
Cipro-Pro 2	1.25	10.0	10.0
Moxifloxacin	0.16	0.16	0.16
Moxi-Pro 1	> 10	> 10	> 10

Fig. 2 Electron microscopy analysis of PdNS-90 (left) and PdNS-170 (right) (A) TEM images, and (B) HAADF–STEM images and corresponding STEM–EDS elemental maps of Pd.

This journal is © The Royal Society of Chemistry 2024

Org. Biomol. Chem., 2024, **22**, 1998–2002 | **1999**

copper grid (Fig. S3 and S4†) confirms the presence of Pd atoms in the nanostructures. Thus, the method using W(CO)$_6$ as a reducing agent could be an alternative to the approach using CO gas for the synthesis of Pd nanosheets.[22]

Prior to testing the catalytic properties of the PdNS in the formation of biofilms, viability assays were performed in cell cultures to test the biocompatibility of the PdNS. Both PdNS-90 and PdNS-170 were found to be fully biocompatible at the concentrations tested (Fig. S5†). Furthermore, we investigated the effect of different nanosheets on the formation of biofilms.

Satisfyingly, low concentrations of the nanosheets displayed no effects on biofilm formation while higher concentrations of 50–100 µg ml^{-1} impaired biofilm buildup (Fig. S6†). This weak antibiotic activity has to be kept in mind for following studies. To compare the catalytic activities of the different nanosheets we used a reporter molecule with a propargylated hydroxy group (4-methyl-7-propargyloxy-coumarin = pro-coumarin)[28] which upon O-propargyl cleavage releases strongly fluorescent 7-hydroxy-4-methylcoumarin (Fig. 3A). Reactions were performed in physiological conditions at 37 °C, either with or without serum. PdNS-90 and PdNS-170 differing in particle size were tested for monitoring fluorescent release kinetics. Both formulations resulted in about 30% release within 4 h suggesting a sufficient speed for liberating the active molecule (Fig. 3B). The release activity was still effective in the presence of 20% serum albeit with reduced kinetics and a cleavage of about 20% after 4 h (Fig. S7†). We next analyzed cleavage of

the prodrugs Cipro-Pro 2 and Moxi-Pro 1 *via* mass-spectrometry (MS) and incubated the prodrugs in PBS (pH = 7.4, isotonicity) at 37 °C.

Analysis of the reactions after 1 h showed that about 50% of Cipro-Pro 2 and 70% of Moxi-Pro 1 consumption, and the simultaneous formation of mass peaks corresponding to the free antibiotics (Fig. S8, and S9†). Given the promising performance in drug release, we loaded agarose hydrogels with Pd nanosheets and tested the prevention of biofilm formation. As both nanosheets exhibited almost similar release kinetics, we selected PdNS-90 for these studies due to their large particle size providing a more stable incorporation into the hydrogel. Various concentrations of Pd nanosheets ranging from 5–50 µg ml^{-1} were embedded in either 1 or 2 mm thick agarose hydrogels (20 mg ml^{-1}) and incubated with Cipro-Pro 2 or Moxi-Pro 1 (5 µM in CASO Medium) for 0–8 h prior to the addition of *S. aureus*. Biofilm formation was monitored after 24 h by CellTiter-Blue™ (Promega) (Fig. S10, and S11†). Overall, while the ciprofloxacin prodrug did not fully inhibit biofilm formation even at highest Pd nanosheet loading and 8 h preincubation, the moxifloxacin prodrug prevented biofilm formation at the highest Pd nanosheet loading, even without preincubation (Fig. 4A). Of note, prolonged incubation of Moxi-Pro 1 for 1 h allowed to reduce the effective Pd-nanosheet concentration to 25 µg ml^{-1} required for abolishing biofilm formation (Fig. 4B). Importantly, the sole incubation with prodrugs or 50 µg ml^{-1} Pd nanosheets loaded hydrogels led only to a minor reduction in biofilm formation. Remarkably, increasing the hydrogel thickness from 1 mm to 2 mm did not influence the overall performance (Fig. 4C). Thus, moxifloxacin prodrug Moxi-Pro 1 and 50 µg ml^{-1} loaded hydrogels of 1 mm thick-
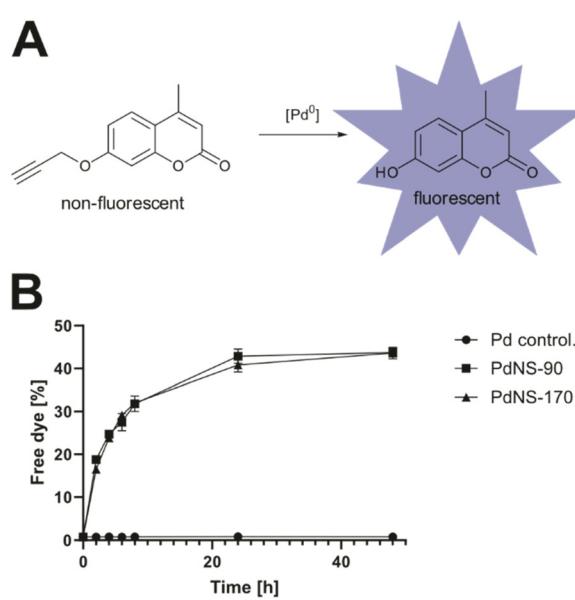

Fig. 3 Comparison of different palladium nanosheets. (A) Principle of the fluorogenic assay used to quantify catalyst activity. (B) Comparison of the catalytic activities of the different palladium nanosheets as determined with the fluorogenic assay (100 µM pro-coumarin, 5 µg ml^{-1} PdNS). The conversion values were calculated from fluorescence intensity measurements at $\lambda_{ex/em}$ = 350/450 nm using a standard curve of the fluorescence intensity of the coumarin. Negative controls: pro-coumarin without nanocatalysts. Error bars: ±SD from n = 3.
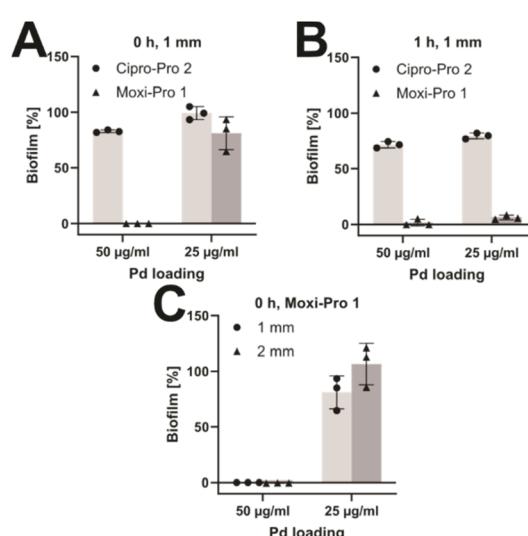

Fig. 4 *In vitro* prevention of Biofilms. (A) Anti-biofilm activity of Cipro-Pro 2 and Moxi-Pro 1 at different Pd-loadings (5 µM prodrug, no pre-incubation). (B) Anti-biofilm activity of Cipro-Pro 2 and Moxi-Pro 1 at different Pd-loadings (5 µM prodrug, 1 h preincubation). (C) Independence of the activation of Moxi-Pro 1 of hydrogel thickness (5 µM prodrug, no preincubation). Error bars: ±SD from n = 3. Full dataset in Fig. S10 and S11.†

2000 | *Org. Biomol. Chem.*, 2024, **22**, 1998–2002

This journal is © The Royal Society of Chemistry 2024

ness represent an optimal coating for implants to prevent biofilms. To test the long-term stability of the catalytic activity we incubated hydrogels loaded with PdNS-90 for several weeks with PBS and exchanged the PBS weekly before visualizing the activity with the fluorogenic assay. A steady decline of the catalytic activity is visible, however after 7 weeks 50% of the original catalytic activity is retained (Fig. S12†). When the medium with prodrug and bacteria was exchanged daily, biofilm development on the coating started on the third day. However, PBS and bacterial growth medium (CASO) both represent extreme, non-physiological conditions. The real situation in tissue is probably somewhere in between these settings.

Catalytic release of active antibiotics from inactive prodrugs is a suitable approach to limit their overall exposure in the body and environment and thus reduce the chance of resistance development. This strategy becomes in particular appealing in the treatment of surface adhered bacteria as the site of antibiotic release is predefined. Pd nanosheet loaded hydrogels demonstrated a proof-of-principle for such a strategy which was exemplarily shown with two marketed fluoroquinolones.

Of note, given the side effects of fluoroquinolones or of other antibiotics by the prodrug approach might be an intriguing perspective to limit toxicity and ensure a safe drug release only at the desired location. As Pd hydrogel were active for several weeks, the strategy is suitable to prophylactically prevent infections on implants directly after their incorporation which represents the most critical phase when bacteria are exposed to the surface and start to adhere.

Author contributions

J.B. and S.A.S. devised the project. M.C.O.L. and A.U.B. developed the nanoparticles, synthesized and characterized them. J. B. synthesized and characterized the prodrugs, tested them in cell culture and for anti-biofilm activity.

Conflicts of interest

The authors declare no conflict of interest.

Acknowledgements

References

1 D. H. Limoli, C. J. Jones and D. J. Wozniak, *Microbiol. Spectrum*, 2015, **3**, DOI: **10.1128/microbiolspec.mb-0011-2014**.

2 C. R. Arciola, D. Campoccia and L. Montanaro, *Nat. Rev. Microbiol.*, 2018, **16**, 397–409.

3 O. Ciofu, E. Rojo-Molinero, M. D. Macia and A. Oliver, *APMIS*, 2017, **125**, 304–319.

4 D. P. Konig, J. M. Schierholz, U. Munnich and J. Rutt, *Arch. Orthop. Trauma Surg.*, 2001, **121**, 297–299.

5 D. Baggio and M. R. Ananda-Rajah, *Aust. Prescr.*, 2021, **44**, 161–164.

6 S. Nadar, T. Khan, S. G. Patching and A. Omri, *Microorganisms*, 2022, **10**, 303.

7 A. D. Verderosa, M. Totsika and K. E. Fairfull-Smith, *Front. Chem.*, 2019, **7**, 824.

8 C. Zhao, L. Zhou, M. Chiao and W. Yang, *Adv. Colloid Interface Sci.*, 2020, **285**, 102280.

9 P. P. Sedghizadeh, S. Sun, A. F. Junka, E. Richard, K. Sadrerafi, S. Mahabady, N. Bakhshalian, N. Tjokro, M. Bartoszewicz, M. Oleksy, P. Szymczyk, M. W. Lundy, J. D. Neighbors, R. G. Russell, C. E. McKenna and F. H. Ebetino, *J. Med. Chem.*, 2017, **60**, 2326–2343.

10 R. Walther, S. M. Nielsen, R. Christiansen, R. L. Meyer and A. N. Zelikin, *J. Controlled Release*, 2018, **287**, 94–102.

11 N. R. Yepuri, N. Barraud, N. S. Mohammadi, B. G. Kardak, S. Kjelleberg, S. A. Rice and M. J. Kelso, *Chem. Commun.*, 2013, **49**, 4791–4793.

12 R. Huang, C.-H. Li, R. Cao-Milán, L. D. He, J. M. Makabenta, X. Zhang, E. Yu and V. M. Rotello, *J. Am. Chem. Soc.*, 2020, **142**, 10723–10729.

13 R. Cao-Milán, S. Gopalakrishnan, L. D. He, R. Huang, L.-S. Wang, L. Castellanos, D. C. Luther, R. F. Landis, J. M. V. Makabenta, C.-H. Li, X. Zhang, F. Scaletti, R. W. Vachet and V. M. Rotello, *Chem*, 2020, **6**, 1113–1124.

14 A. Nabawy, R. Huang, D. C. Luther, X. Zhang, C. H. Li, J. M. Makabenta and V. M. Rotello, *Chem. Sci.*, 2022, **13**, 12071–12077.

15 J. T. Weiss, J. C. Dawson, K. G. Macleod, W. Rybski, C. Fraser, C. Torres-Sanchez, E. E. Patton, M. Bradley, N. O. Carragher and A. Unciti-Broceta, *Nat. Commun.*, 2014, **5**, 3277.

16 R. M. Yusop, A. Unciti-Broceta, E. M. Johansson, R. M. Sanchez-Martin and M. Bradley, *Nat. Chem.*, 2011, **3**, 239–243.

17 A. Unciti-Broceta, E. M. Johansson, R. M. Yusop, R. M. Sanchez-Martin and M. Bradley, *Nat. Protoc.*, 2012, **7**, 1207–1218.

18 A. M. Perez-Lopez, B. Rubio-Ruiz, T. Valero, R. Contreras-Montoya, L. Alvarez de Cienfuegos, V. Sebastian, J. Santamaria and A. Unciti-Broceta, *J. Med. Chem.*, 2020, **63**, 9650–9659.

19 J. T. Weiss, N. O. Carragher and A. Unciti-Broceta, *Sci. Rep.*, 2015, **5**, 9329.

This journal is © The Royal Society of Chemistry 2024

Org. Biomol. Chem., 2024, **22**, 1998–2002 | **2001**

20 A. M. Perez-Lopez, B. Rubio-Ruiz, V. Sebastian, L. Hamilton, C. Adam, T. L. Bray, S. Irusta, P. M. Brennan, G. C. Lloyd-Jones, D. Sieger, J. Santamaria and A. Unciti-Broceta, *Angew. Chem., Int. Ed.*, 2017, **56**, 12548–12552.

21 B. Rubio-Ruiz, J. T. Weiss and A. Unciti-Broceta, *J. Med. Chem.*, 2016, **59**, 9974–9980.

22 M. Sancho-Albero, B. Rubio-Ruiz, A. M. Pérez-López, V. Sebastián, P. Martín-Duque, M. Arruebo, J. Santamaría and A. Unciti-Broceta, *Nat. Catal.*, 2019, **2**, 864–872.

23 M. C. Ortega-Liebana, N. J. Porter, C. Adam, T. Valero, L. Hamilton, D. Sieger, C. G. Becker and A. Unciti-Broceta, *Angew. Chem., Int. Ed.*, 2022, **61**, e202111461.

24 C. Adam, T. L. Bray, A. M. Pérez-López, E. H. Tan, B. Rubio-Ruiz, D. J. Baillache, D. R. Houston, M. J. Salji, H. Y. Leung and A. Unciti-Broceta, *J. Med. Chem.*, 2022, **65**, 552–561.

25 H. Chen, R. Feng, T. Xia, Z. Wen, Q. Li, X. Qiu, B. Huang and Y. Li, *Gels*, 2023, **9**, 423.

26 Y. Li, Y. Yan, Y. Li, H. Zhang, D. Li and D. Yang, *CrystEngComm*, 2015, **17**, 1833–1838.

27 S. Ando, E. Yamamoto, M. Kobayashi, A. Kumatani and M. Osada, *ACS Nano*, 2024, **18**(1), 461–469.

28 X.-P. Zhang, Q. Yuan, Y.-L. Qi, D.-J. Zheng, Q.-X. Liu, B.-Z. Wang, Y.-S. Yang and H.-L. Zhu, *Spectrochim. Acta, Part A*, 2019, **220**, 117134.

2002 | *Org. Biomol. Chem.*, 2024, **22**, 1998–2002

This journal is © The Royal Society of Chemistry 2024